Electronic Supplementary Material (ESI) for Chemical Science.

Supplementary Materials for

Heterogeneous Electron Transfer Reorganization Energy at Inner Helmholtz Plane in a Polybromide Redox-Active Ionic Liquid

Moonjoo Kim[1§], Sangmee Park[2§], and Taek Dong Chung[1,2*]

[1] *Department of Chemistry, Seoul National University, Seoul 08826, South Korea*

[2] *Program in Nano Science and Technology, Advanced Institute of Convergence Technology, Seoul National University, Suwon-Si, Gyeonggi-do 16229, South Korea*

[§] Both authors contributed equally to this work

[*] Corresponding author: Prof. Taek Dong Chung, tdchung@snu.ac.kr

1. Methods

1.1. Chemicals

1-ethyl-1-methylpyrrolidinium bromide (MEPBr, >99 %), 1-butyl-1-methylpyrrolidinium bromide (MBPBr, >99 %), potassium phosphate monobasic (KH_2PO_4, ≥99.0%), potassium phosphate dibasic (K2HPO4, ≥98%), titanium(III) chloride solution ($TiCl_3$, 12% Ti in HCl solution) and sodium bicarbonate ($NaHCO_3$, 99.7-100.3%) was purchased from Sigma-Aldrich. Phosphoric acid (H_3PO_4, 85%) was purchased from Acros Organics. All chemicals were used as received. All solutions were prepared with Milli-Q deionized water.

1.2. Synthesis of Polybromide Ionic Liquids

1-ethyl-1-methylpyrrolidinium polybromide ($MEPBr_{2n+1}$) was electrochemically synthesized in a three-electrode system in 250 mM MEPBr aqueous, 1 M potassium phosphate buffer solution as previously reported.[1] A Compactstat potentiostat (Ivium Technologies) and PGSTAT302N (Metrohm AG) were used for electrochemical measurements. Ag/AgBr (3 M KBr) and Pt wire were used as a reference electrode and a counter electrode, respectively. Pt macroelectrode was used as the working electrode, and the diameter of Pt exposed to the solution was longer than 3 mm. 1.2 V vs Ag/AgBr was applied overnight to synthesize $MEPBr_{2n+1}$ droplet. The droplet was dark orangish-brown and several mm in size. 1-butyl-1-methylpyrrolidinium polybromide ($MBPBr_{2n+1}$) was synthesized using the same method.

1.3. Electrochemical Measurements

A Compactstat potentiostat (Ivium Technologies), PGSTAT302N (Metrohm AG) or CHI 660E (CH Instruments) was used for electrochemical measurements. A Pt or carbon ultramicroelectrode (UME) dipped into the synthesized $MEPBr_{2n+1}$ droplet was used as a working electrode. All UMEs were purchased from commercial vendors (CH Instruments, BASi and Metrohm AG). The contact between the UME and $MEPBr_{2n+1}$ was confirmed via the change of the open circuit potential. UMEs were mechanically polished with the silicon carbide grinding paper (CarbiMet) before the electrochemical measurements. The reference electrode is either Ag/AgBr (3M KBr) or the Pt macroelectrode used as working electrode during $MEPBr_{2n+1}$ synthesis. Fig. S1a illustrates the electrochemical set-up. Since the area of the $MEPBr_{2n+1}$/aqueous solution interface was 3-5 orders larger than the size of the UME, impedance at the interface was negligible[1] (see Fig. S1b).

1.4. Preparation of TiO_2 Deposited Pt UME

TiO_2-modified Pt electrodes (TiO_2@Pt) were prepared using a method described in the previous report.[2] To briefly introduce the method, a precursor solution for TiO_2 deposition was prepared by diluting the 12% $TiCl_3$ solution in deionized water with a ratio of 1:20. Then, the solution was neutralized to the pH 2.45 ± 0.03 by slow addition of 0.6 M $NaHCO_3$ solution. The electrodeposition was performed by applying 64 mV vs Ag/AgCl (3 M KCl) on a Pt UME immersed in a freshly prepared $TiCl_3$ solution. The TiO_2 coverage (θ_{TiO2}) of TiO_2@Pt is calculated from the difference in hydrogen underpotential deposition charges before and after electrodeposition of TiO_2.

1.5. Fit for CV data to the Butler-Volmer (BV) model

CV was converted to overpotential–current data by taking the potential of the minimum current as an equilibrium potential. Exchange current (i_0) and transfer coefficient(α) were respectively calculated from the y-intercept of the Tafel plot and the Tafel slope. Then, the data was fitted to the BV model using i_0 and α. The steady-state mass transport limited BV equation was used for the Fig. 2b, and the BV equation without mass transport limit, $i = i_0\left[e^{(1-\alpha)f\eta} - e^{-\alpha f\eta}\right]$, was used for the Fig. 3.

1.6. Electrochemical Impedance Spectroscopy (EIS)

A Gamry potentiostat was used for measuring impedance spectra of electrode–$MEPBr_{2n+1}$ interfaces. Pt UME or TiO_2@Pt UME dipped in $MEPBr_{2n+1}$ served as a working electrode. The reference electrode was the Pt macroelectrode which was working electrode during $MEPBr_{2n+1}$ synthesis (see Fig. S1a). The EIS experiments were carried out at different working electrode dc potentials superimposed by an ac potential of 5 mV rms. The frequency range was extended from 1 kHz to 500 kHz with 10 points per decade. The impedance spectra were fitted to the Randles circuit with spherical diffusion Warburg using the MEISP software.[1]

2. Derivation of a Current-Overpotential Equation for MHC Model

Since the electrochemical rate constant for the MHC model in equation (6) is mathematically difficult to be employed, Bazant *et al.* reported an analytical approximation of the equation. A reduction rate constant, k_{red} and an oxidation rate constant, k_{ox} in the simple formula for the MHC model is expressed as follows when $\lambda^* \gg 1$:[3]

$$k_{red}(\lambda^*, E^*) = Z \cdot \frac{\sqrt{\pi\lambda^*}}{1 + \exp(E^* - E^{0,*})} \cdot \operatorname{erfc}\left(\frac{\lambda^* - \sqrt{1 + \sqrt{\lambda^*} + (E^* - E^{0,*})^2}}{2\sqrt{\lambda^*}}\right) \tag{S1}$$

$$k_{ox}(\lambda^*, E^*) = Z \cdot \frac{\sqrt{\pi\lambda^*}}{1 + \exp(-(E^* - E^{0,*}))} \cdot \operatorname{erfc}\left(\frac{\lambda^* - \sqrt{1 + \sqrt{\lambda^*} + (E^* - E^{0,*})^2}}{2\sqrt{\lambda^*}}\right) \tag{S2}$$

Where λ is reorganization energy, E is the electrode potential, E^0 is the standard potential, Z is the pre-exponential factor, and the superscript * denotes normalization to the thermal voltage as shown in equation (S3).

$$\lambda^* = \frac{\lambda}{k_B T} \tag{S3}$$

where, k_B is the Boltzmann constant, and T is temperature.

However, the simple formula suggested by Bazant *et al.* cannot be directly applied to fit the experimental data because both Z and E^0 of Br_2 reduction in $MEPBr_{2n+1}$ are unknown. Thus, we constructed a current-overpotential equation for the MHC model along coordinates of current normalized by exchange current ($^{i}/_{i_0}$) and overpotential ($\eta = E - E_{eq}$).

According to Faraday law, the current for one electron-transfer is as follows:

$$\frac{i(E)}{FA} = k_{ox}C_R - k_{red}C_O \tag{S5}$$

where C_i is the concentration of redox-active species, F is Faraday constant, and A is electrode surface area. Assuming that the rate-determining step for the current is not mass transport of redox-active species, but electron transfer between electrode-electrolyte interface, concentrations of redox-active species at the electrode surface are the same as those in the bulk. Under this condition, the Nernst equation is expressed as follows:

$$E_{eq} = E^0 - \frac{RT}{F}\ln\frac{C_R}{C_O} \tag{S6}$$

Let $c^* = \left(E_{eq} - E^0\right)\cdot {}^{F}\!/_{RT} = E^*_{eq} - E^{0,*}$.

$$\frac{C_O}{C_R} = \exp(c^*) \tag{S7}$$

Substituting equation (S1) – (S2) and (S7) into equation (S5) yields equation (S8).

$$\frac{i(E)}{ZFAC_R} = \sqrt{\pi\lambda^*}\cdot \operatorname{erfc}\left(\frac{\lambda^* - \sqrt{1+\sqrt{\lambda^*}+(\eta^*+c^*)^2}}{2\sqrt{\lambda^*}}\right)\left(\frac{\exp(\eta^*)-1}{\exp(\eta^*)+\exp(-c^*)}\right) \tag{S8}$$

where $\eta^* = \eta\cdot {}^{e}\!/_{k_BT} = (E^* - E^{0,*})$. e is the elementary charge

Exchange current can be expressed as follows:

$$\frac{i_0}{ZFAC_R} = \operatorname{erfc}\left(\frac{\lambda^* - \sqrt{1+\sqrt{\lambda^*}+c^{*2}}}{2\sqrt{\lambda^*}}\right)\left(\frac{\sqrt{\pi\lambda^*}}{1+\exp(-c^*)}\right) \tag{S9}$$

Organizing equation (S8) and (S9) yields equation (S10) which is the current-overpotential equation for the MHC kinetics.

$$\frac{i(E)}{i_0} = \frac{\operatorname{erfc}\left(\frac{\lambda^* - \sqrt{1+\sqrt{\lambda^*}+(\eta^*+c^*)^2}}{2\sqrt{\lambda^*}}\right)}{\operatorname{erfc}\left(\frac{\lambda^* - \sqrt{1+\sqrt{\lambda^*}+c^{*2}}}{2\sqrt{\lambda^*}}\right)}\left(\frac{\exp(\eta^*)-1}{\exp(\eta^*)+\exp(-c^*)}\right)(1+\exp(-c^*)) \tag{S10}$$

Reorganization energy was calculated by fitting $\log(i/i_0)$ vs η data from 0 V to −0.6 V vs E_{eq} to equation (S9) using MATLAB with fitting parameters of λ^* and c^*. i_0 was calculated using the Tafel plot analysis. λ of this work (λ^* higher than 7.5) is large enough to satisfy the assumption of the simple formula for the MHC model, equation (S1−S2).

3. Electrochemical Cell

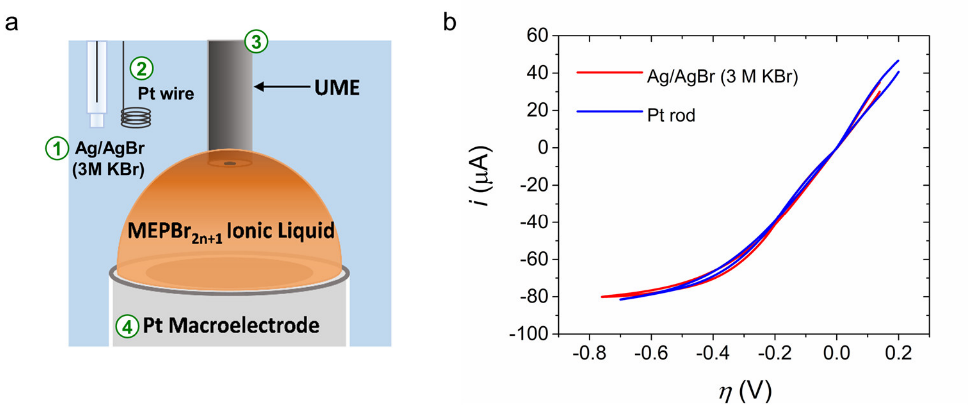

Fig. S1. Experimental Scheme. (a) Illustration of electrochemical measurements set-up where an UME is dipped in the MEPBr$_{2n+1}$ droplet that was electrochemically synthesized at ④ Pt macroelectrode in 250 mM MEPBr, 1 M potassium phosphate buffer aqueous solution. (b) CVs in MEPBr$_{2n+1}$ with pH 3 phosphate buffer at Pt UME (diameter 50 μm). Scan rate is 10 mV/s. The red line is measured when a reference electrode was ① Ag/AgBr (3 M KBr), and a counter electrode was ② Pt wire. Both electrodes were located in the aqueous solution as depicted in Fig. S1a. The blue line is measured when ④ Pt macroelectrode was utilized as both a reference electrode and a counter electrode. This result indicates that the interfacial impedance between MEPBr$_{2n+1}$ and the aqueous solution is negligible.

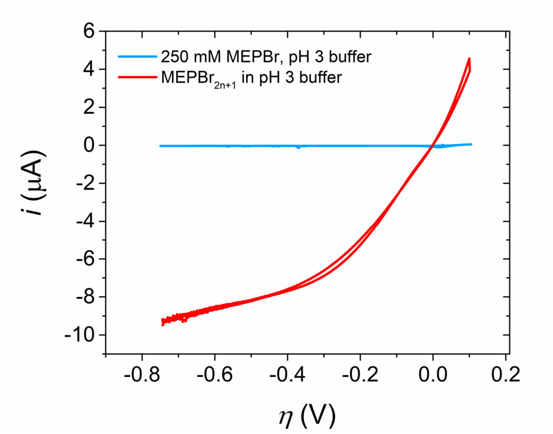

Fig. S2. CVs at Pt UME in 250 mM MEPBr, pH 3, 1 M potassium phosphate buffer solution at 100 mV/s (blue) and in MEPBr$_{2n+1}$ which was electrochemically synthesized in 250 mM MEPBr, pH 3, 1 M potassium phosphate buffer solution at 10 mV/s (red).

4. Potential of zero charge (PZC) of Pt and TiO_2@Pt in $MEPBr_{2n+1}$

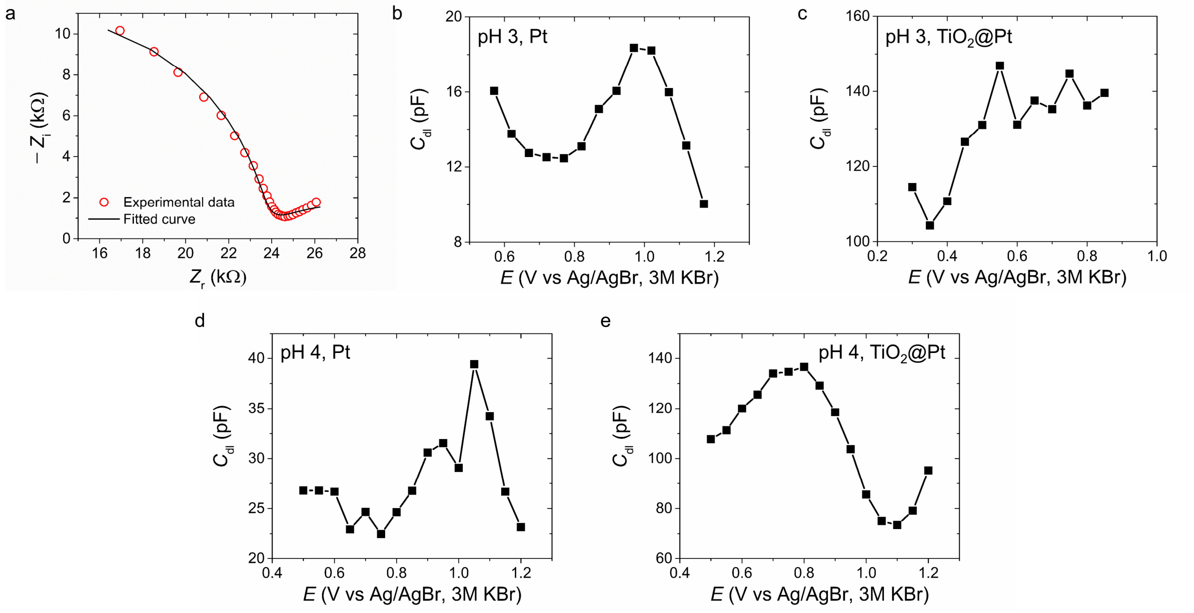

Fig. S3. EIS analysis of Pt and TiO_2@Pt in $MEPBr_{2n+1}$. (a) Representative Nyquist plot of Pt UME in $MEPBr_{2n+1}$ (red dots, frequency decreases from left to right) and its fit to the Randles circuit with spherical diffusion Warburg (black line). The left semicircle shows the charge transfer resistance and double layer capacitance. (b-d) The fitted double-layer capacitance (C_{dl}) as a function of electrode dc potentials at (b, d) Pt UME and (c, e) TiO_2@Pt with a θ_{TiO2} of 0.55 in $MEPBr_{2n+1}$ at (b-c) pH 3 and (d-e) pH 4.

We performed EIS at Pt and TiO_2@Pt in $MEPBr_{2n+1}$ and fitted EIS to the Randles circuit with spherical diffusion Warburg.[1] EIS has been employed to measure PZC of electrodes in ionic liquids.[4–6] Electric double layer (EDL) structure of ionic liquids cannot be explained by classical Gouy–Chapman–Stern theory which predicts the minimum C_{dl} at PZC in diluted solution. Alternatively, ionic liquids have local maximum C_{dl} around PZC because crowded ions in the EDL of ionic liquids block further charging.[7] Correspondingly, C_{dl}–E of Pt and TiO_2@Pt in $MEPBr_{2n+1}$ (Fig. S3b-e) have bell-shaped curve while the potential of local maximum C_{dl} is assigned to PZC. PZC of Pt UME is 1.05 V in both $MEPBr_{2n+1}$ at pH 3 and pH 4, and PZC of TiO_2@Pt (θ_{TiO2}) is 0.55 V and 0.85 V in $MEPBr_{2n+1}$ at pH 3 and pH 4, respectively.

5. Supplementary Tables

	Pt UME	**Carbon UME**
Tafel slope (mV/decade)	139 ± 5	113 ± 13
Exchange Current, i_0 (nA)	777 ± 207	3.78 ± 0.64
Transfer coefficient, α	0.43 ± 0.02	0.53 ± 0.06

Table S1. Tafel slope, exchange current, and transfer coefficient extracted from the Tafel plot of Pt UME and carbon UME ($n = 4$).

	pH 3	**pH 4**
Reorganization energy (meV)	196 ± 21	197 ± 13

Table S2. Mean and standard deviation of reorganization energies of Pt UME measured in $MEPBr_{2n+1}$ in 1 M phosphate buffers at pH 3 and 4.

	$MEPBr_{2n+1}$	**$MBPBr_{2n+1}$**
Reorganization energy (meV)	196 ± 21 ($n = 32$)	186 ± 17 ($n = 18$)

Table S3. Mean and standard deviation of reorganization energies of Pt UME measured in $MEPBr_{2n+1}$ and $MBPBr_{2n+1}$ at pH 3, 1 M phosphate buffers. T test with unequal variances leads that two datasets have none-equal averages in 90 % confidence level.

References

1 S. Park, D. H. Han, J. G. Lee and T. D. Chung, *ACS Appl. Energy Mater.*, 2020, **3**, 5285–5292.

2 D. Eisenberg, H. S. Ahn and A. J. Bard, *J. Am. Chem. Soc.*, 2014, **136**, 14011–14014.

3 Y. Zeng, R. B. Smith, P. Bai and M. Z. Bazant, *J. Electroanal. Chem.*, 2014, **735**, 77–83.

4 V. Lockett, M. Horne, R. Sedev, T. Rodopoulos and J. Ralston, *Phys. Chem. Chem. Phys.*, 2010, **12**, 12499–12512.

5 M. Drüschler, B. Huber, S. Passerini and B. Roling, *J. Phys. Chem. C*, 2010, **114**, 3614–3617.

6 M. Drüschler, B. Huber and B. Roling, *J. Phys. Chem. C*, 2011, **115**, 6802–6808.

7 M. V. Fedorov and A. A. Kornyshev, *Chem. Rev.*, 2014, **114**, 2978–3036.